Biosensors and Bioelectronics 145 (2019) 111702

Contents lists available at ScienceDirect

Biosensors and Bioelectronics

journal homepage: www.elsevier.com/locate/bios

Wavelength distinguishable signal quenching and enhancing toward photoactive material 3,4,9,10-perylenetetracarboxylic dianhydride for simultaneous assay of dual metal ions

Liaojing Huang, Hanmei Deng, Xia Zhong, Minghui Zhu, Yaqin Chai, Ruo Yuan**, Yali Yuan*

Key Laboratory of Luminescent and Real-Time Analytical Chemistry (Southwest University), Ministry of Education, College of Chemistry and Chemical Engineering, Southwest University, Chongqing, 400715, PR China

ARTICLE INFO

Keywords:
Photoelectrochemical biosensor
Wavelength distinguishable
Simultaneous multiplex assay
Signal quenching and enhancing

ABSTRACT

Photoelectrochemical (PEC) assay with low background, simple instrumentation and high sensitivity has deemed as one of the most potential strategies to simultaneous multi-component detection. How to distinguish photocurrent changes caused by various targets on a single sensing platform thus becomes the key issue to be resolved. Herein, we innovatively proposed a multiplex PEC biosensor based on wavelength distinguishable signal quenching and enhancing toward photoactive material 3,4,9,10-perylenetetracarboxylic dianhydride (PTCDA) for simultaneous assay of dual metal ions. Briefly, S1 and S2 ssDNA containing sensitizer methylene blue and quencher ferrocene (termed as MB-S1 and Fc-S2), respectively, were first generated through target Pb^{2+} and Mg^{2+}-induced DNAzyme-assisted target recycling, which thereafter were modified on PTCDA sensing platform specifically via host-guest recognition with β-cyclodextrin (β-CD). Interestingly, the sensitizer MB could enhance photocurrent of PTCDA under the excitation wavelength of 623 nm and 590 nm, respectively, while the quencher Fc just quencher the photocurrent of PTCDA under the excitation wavelength of 590 nm, thereby achieving wavelength distinguishable signal quenching and enhancing toward photoactive material PTCDA for simultaneous assay of dual metal ions. As a result, the conceived biosensor for Mg^{2+} and Pb^{2+} detection realized high sensitivity with detection limit of 0.3 pM and 0.3 nM, respectively. The proposed strategy not only for the first time achieved the discrimination of varied PEC signal caused by two targets with usage of sole photoelectric material, but also realized the simultaneous multiplex assay on a single sensing platform, providing a new way for constructing effective and sensitive PEC biosensor for multi-component detection.

1. Introduction

The concentration of metal ions is intensively relevant to the natural function of human body. For example, the overdose of Mg^{2+} and Pb^{2+} would lead to the renal function losses with serious kidney disease. Accordingly, it is essential to exploit simple and effective approaches to realize their ultra-trace detection. In response, many multiplex simultaneous assays based on electrochemistry (EC) (Li et al., 2018; Lu et al., 2019; Miao et al., 2017; Tang et al., 2018), microfluidic chip (Li et al., 2017), NMR spectroscopy (Bar-Shir et al., 2015; Tassali et al., 2014), plasma-induced vapor generation (Liu et al., 2019), surface-enhanced Raman scattering (SERS) (Shi et al., 2018), fluorescent (FL) (Li et al., 2015; Shen et al., 2017; Yun et al., 2017), calorimetry (Chen et al., 2019) et al., have thus been established with the utilizing of different signal probes. However, photoelectrochemistry (PEC) (Huang et al., 2018b; Yang et al., 2019; Zeng et al., 2019a, 2019b; Zhang et al., 2019; Zhu et al., 2019), an emerging and valuable analytical technique with low background, simple instrumentation and high sensitivity, was rarely applied for multiplex assay because of the challenge in distinguishing photocurrent changes caused by different targets.

In PEC sensing system, the photoactive material is the key factor for signal generation and the photocurrent intensity mainly depends on the applied bias voltage, excitation wavelength and composition of electrolyte solution (Guo et al., 2019), thereby providing the possibility for distinguishing different targets related photocurrent changes on the basis of potentiometric addressable (Dai et al., 2016), light addressable (Wang et al., 2015, 2017), wavelength resolved (Deng et al., 2019; Zheng et al., 2016) and electron donors/acceptors (D/A) resolved strategies. Although the success in multi-component detection, most of the reported PEC strategies were difficult to achieve simultaneous assay

* Corresponding author.
** Corresponding author.
E-mail addresses: yuanruo@swu.edu.cn (R. Yuan), y198688@swu.edu.cn (Y. Yuan).

https://doi.org/10.1016/j.bios.2019.111702
Received 17 July 2019; Received in revised form 9 September 2019; Accepted 13 September 2019
Available online 13 September 2019
0956-5663/

on a single sensing surface owing to the inconvenience change of detection condition toward different targets. In comparison, the change of excited light wavelength can be implemented by a simple programming, and thus showing desirable prospect in multiplex simultaneous assay. In this view, our group fabricated the wavelength-resolved PEC biosensor with targets related two photoactive materials generating varied photocurrent signals at different wavelengths on a single interface for multiplex simultaneous assay (Deng et al., 2019; Zheng et al., 2016), which however suffered from the fussy operation process and limited sensitivity owing to the labeling of small amounts of diverse signal probes. If sole photoactive material can accomplish the multiplex simultaneous assay, the operability and sensitivity might be improved to a certain extent, however, there was no relevant work reported to the best of our knowledge.

3,4,9,10-perylenetetracarboxylic dianhydride (PTCDA) is a polyaromatic organic pigment containing the amounts of perylene and ambient rich oxygen elements (Wang et al., 2016) and can generate PEC signal both at the excitation wavelength of 623 nm and 590 nm (Huang et al., 2018a). Interestingly, we found that the sensitizer methylene blue (MB) could significantly enhance the photocurrent of PTCDA under the excitation wavelength of 623 nm and 590 nm, respectively, while the quencher ferrocene (Fc) just quencher the photocurrent of PTCDA under the excitation wavelength of 590 nm. Inspired by this, we for the first time constructed a multiplex PEC biosensor based on wavelength distinguishable signal quenching and enhancing toward photoactive material PTCDA for simultaneous assay of dual metal ions. As shown in Scheme 1, MB-S1 and Fc-S2 ssDNA derived from target Pb^{2+} and Mg^{2+}-induced DNAzyme-assisted target recycling respectively were modified on PTCDA sensing platform specifically via typical host-guest recognition with β-CD (Agnihotri et al., 2015; Jiang et al., 2018; Wang et al., 2019; Wu et al., 2019), and thus achieving the wavelength distinguishable signal quenching and enhancing toward sole photoactive material PTCDA for simultaneous assay of dual metal ions. Moreover, since the PTCDA possessed well film-forming property, the immobilization amount of PTCDA could be improved significantly and fussy labeling process would be avoided, thereby providing a new way for constructing effective and sensitive PEC biosensor for multi-component detection and holding a great application prospect in biological monitoring.

2. Experimental methods

2.1. Reagents and materials

3,4,9,10-perylenetetracarboxylic dianhydride (PTCDA) was purchased from Lian Gang Dyestuff Chemical Industry Co., Ltd. (Liaoning, China). Amino modified β-cyclodextrin (β-CD) was bought from Aladdin (Shanghai, China). Amino modified-Magnetic nanoparticles (Fe_3O_4, 100 mg mL^{-1}) was obtained from Tianjin Base Line Chrome Tech Research Centre (Tianjin, China). L-Cysteine (L-Cys) was prepared by J&K Scientific Co., Ltd. (Beijing, China). Tris-HCl buffer (pH 7.4) containing 20 mM Tris-HCl, 140 mM NaCl, 5 mM KCl and 1 mM $CaCl_2$ was applied to dilute DNA. All oligonucleotides used in this work were purchased from Sangon Biotech Co., Ltd. (Shanghai, China), and the corresponding sequences were displayed as follows (from 5′ to 3′):

Pb^{2+}-substrate strand (Pb-Sub): SH-$(CH_2)_6$ GCA TAC TCA CTA T/rA/G GAA GAG ATG-MB

Pb^{2+}-catalysis strand (Pb-Cata): CAT CTC TTC TCC GAG CCG GTC GAA ATA GTG AGT ATG C

Mg^{2+}-substrate strand (Mg-Sub): SH-$(CH_2)_6$ AAT CTG CAG AGT AT/rA/ GGA TAT CC-Fc

Mg^{2+}-catalysis strand (Mg-Cata): GGA TAT CAG CGA TCA CCC ATG TTA CTC TGC AGA TT

2.2. Apparatus

The photoelectrochemical (PEC) measurements were realized through a PEC workstation (Ivium, Netherlands) and measured in PBS (pH 7.0) including 0.1 M ascorbic acid (AA) under 0.0 V (vs SCE) with a light-emitting diode (LED) lamp irradiation for 10-20-10 s. Electrochemical impedance spectroscopy (EIS) measurements were performed by a CHI 660e electrochemical workstation (Shanghai Chenhua Instrument Co., Ltd., China). EIS was performed in 5 mM $[Fe(CN)_6]^{3-/4-}$ (pH 7.0) (frequency range: 0.1–100 kHz, amplitude: 5 mV).

2.3. Pb^{2+} and Mg^{2+}-induced DNAzyme-assisted target recycling

First, 5 mL 16 nm gold nanoparticles (nano-Au) (Frens, 1973) was added to 1 mL purified Fe_3O_4 and stirred for 2 h to obtain the nano-Au functionalized magnetic nanocomposites (Au@Fe_3O_4), which subsequently rinsed several times and redispersed in 2 mL ultrapure water. Then, 10 μL Subs (Pb-Sub and Mg-Sub, 5 μM, respectively), on which sensitizer methylene blue (MB) and quencher ferrocene (Fc) was respectively modified at the DNA terminus, were mixed with 10 μL Au@Fe_3O_4 magnetic nanocomposites and stirred over 12 h at 4° C. After that, the mixture was magnetically separated in order to eliminate excess Subs. To form Pb^{2+} and Mg^{2+}-dependent DNAzymes, 10 μL Enzs (Pb-Enz and Mg-Enz, 2.5 μM, respectively) were added to above mixture and stir for 2 h at 4° C. Thereafter, the target Pb^{2+} or Mg^{2+} with various concentrations was introduced into solution. Since the Pb^{2+} and Mg^{2+} can specially shear the corresponding binding site of Pb^{2+} and Mg^{2+}-dependent DNAzymes, the MB-Sub and Fc-Sub ssDNA related to target Pb^{2+} and Mg^{2+} can be acquired through incubation of 2 h.

2.4. Fabrication of the proposed biosensor

The cleaned glassy carbon electrode (GCE, $\Phi = 4$ mm) (Zhuang et al., 2015) was incubated with 3 μL 4 mM PTCDA and dried 12 h at room temperature. Then, the modified electrode was immersed in 1% $HAuCl_4$ at −0.2 V for 30 s to acquire an Au nanoparticle (depAu) layer, which could thus heighten the electronic transmission efficiency through SPR effect of depAu and offer plentiful binding sites for subsequent immobilization. Following that, the electrode was coated with 10 μL 1 mM β-CD and incubated for 12 h at 4 C. Finally, the generated MB-S1 and Fc-S2 from Pb^{2+} or Mg^{2+}-induced DNAzyme-assisted target recycling were dropped on the electrode for 40 min reaction at room temperature. MB-S1 and Fc-S2, which respectively related to the concentration of Pb^{2+} or Mg^{2+} could be captured on surface of the electrode through host-guest recognition, thereby affecting the photocurrent of PTCDA to achieve highly sensitive and effective detection of Pb^{2+} and Mg^{2+} simultaneously.

3. Results and discussion

3.1. Detection principle of the PEC biosensor

The detection principle was shown in Scheme 1. Concretely, the sensitization of MB toward PTCDA could be explained as: the photons received from 623 nm and 590 nm both increased due to the augmented light absorption range of MB (Scheme 1). The principle that Fc annihilated photocurrent signal of PTCDA may was that the empty orbit of Fc would capture the light-generated electrons, and the amount of light-generated electrons by PTCDA at 590 nm was much more than 623 nm (Scheme 1). Therefore, after Fc was trapped on the surface of PTCDA, the photocurrent signal was significantly reduced at 590 nm and remained almost unchanged at 623 nm. From this perspective, the change of photocurrent signal at 623 nm was proportional to the concentration of MB, while the variety of photocurrent signal at 590 nm was influenced by the concentrations of MB and Fc at the same time. Therefore,

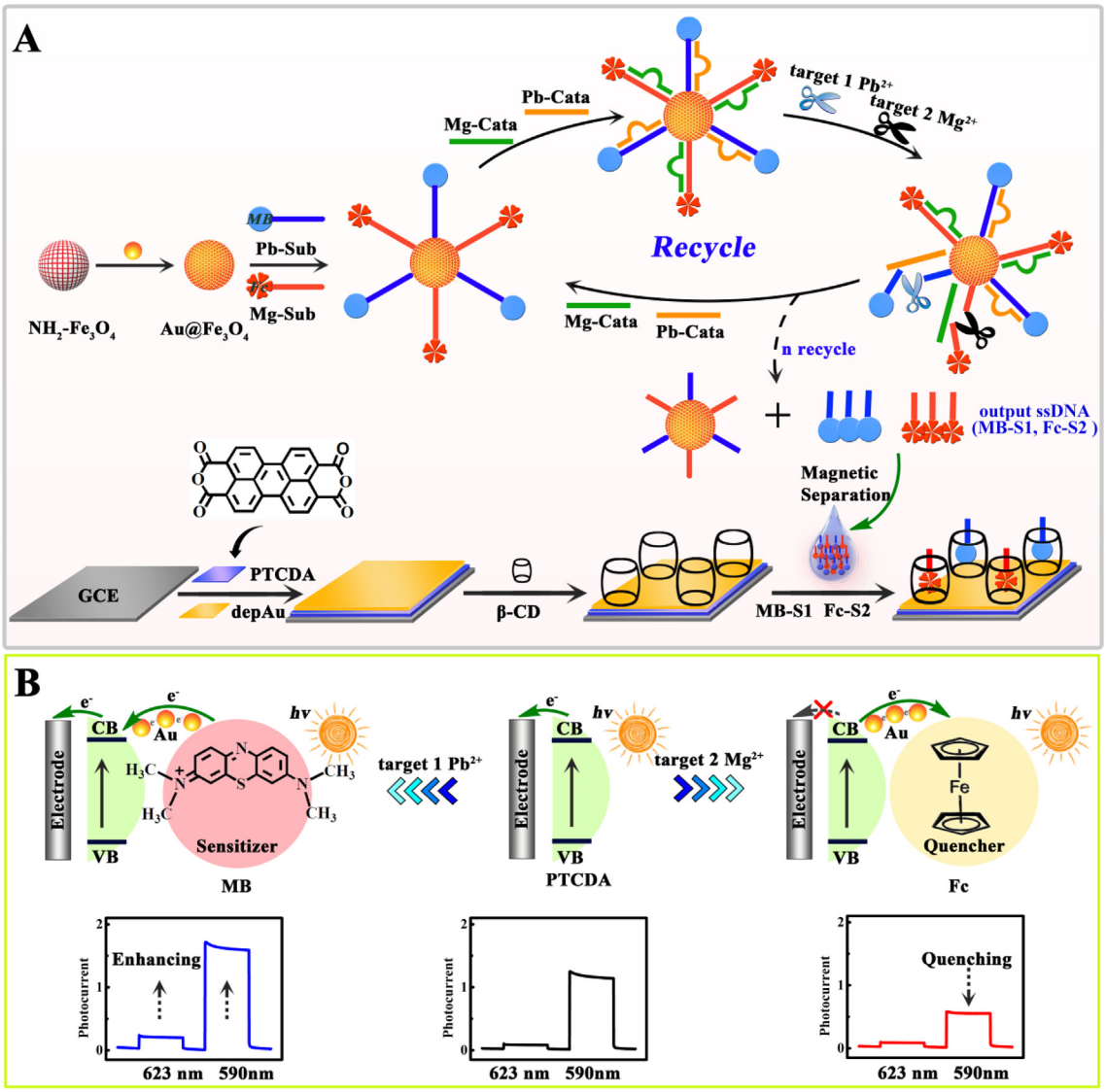

Scheme 1. (A) Schematic illustration of the multiplex PEC biosensor based on wavelength distinguishable signal quenching and enhancing toward photoactive material PTCDA for simultaneous assay of Mg^{2+} and Pb^{2+}; (B) the quenching and enhancing mechanisms toward photoactive material PTCDA.

the MB concentration could be calculated by the change of photocurrent signal at 623 nm, and the obtained concentration of MB could be used to compute the photocurrent increment of MB to PTCDA at 590 nm, then the remaining signal at 590 nm was utilized to calculate the concentration of Fc.

3.2. PEC and EIS characterization of the biosensor

To trace the assembly process, we monitored PEC response of the stepwise fabricated electrodes (Fig. 1). As shown in Fig. 1A, there was no obvious photocurrent signal (curve a) at the bare GCE. After the PTCDA was modified on GCE, a strong PEC signal was observed (curve b), indicating that PTCDA was a desirable photoelectric material. After depositing the electrode with depAu layer, the PEC signal increased (curve c) because of its excellent electron transfer capability. Subsequently, the PEC response decreased after incubating the electrode with inert β-CD (curve d). Ultimately, after modification of the β-CD/depAu/PTCDA/GCE with Fc-S2, PEC signal at 590 nm was decreased (curve e), manifesting that Fc could act as quencher to effectually decrease the photocurrent of PTCDA at 590 nm. However, after assembly of the β-CD/depAu/PTCDA/GCE with MB-S1, remarkably increased PEC signal at 623 nm and 590 nm was recorded (curve f), implying that MB could act as sensitizer to efficiently enhance the photocurrent of PTCDA.

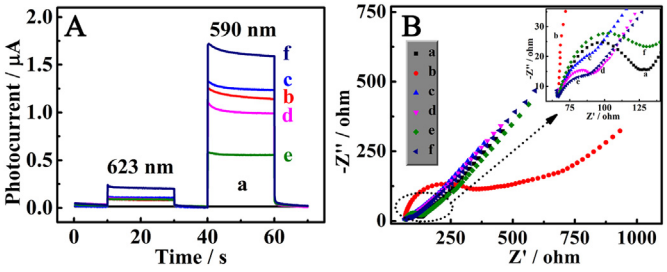

Fig. 1. (A) PEC profiles in PBS 7.0 containing 80 mM L-Cys and (B) EIS profiles in 5.0 mM $[Fe(CN)_6]^{3-/4-}$ toward 100 nM Mg^{2+} and 500 nM Pb^{2+} of each modified electrode: (a) bare GCE, (b) PTCDA/GCE, (c) depAu/PTCDA/GCE, (d) β-CD/depAu/PTCDA/GCE, (e) Fc-S2/β-CD/depAu/PTCDA/GCE and (f) MB-S1/β-CD/depAu/PTCDA/GCE.

Moreover, to further confirm the stepwise modification of PEC biosensor, the electrochemical technique was utilized in 5.0 mM $[Fe(CN)_6]^{3-/4-}$ by EIS. As displayed in Fig. 1B, the bare GCE exhibited a small EIS value (curve a). Then, EIS value increased (curve b) after assembly of semiconductor PTCDA on GCE electrode. Subsequently,

after depositing depAu layer on the electrode, EIS value decreased (curve c) owing to its superior conductivity. Afterwards, EIS value increased (curve d) after introduction of inert β-CD on electrode. Finally, when the β-CD/depAu/PTCDA/GCE was incubated with Fc-S2, a slightly decreased impedance value was observed owing to the existence of quencher Fc with redox activity (curve e). Nevertheless, after capturing MB-S1 on the β-CD/depAu/PTCDA/GCE, an enhanced impedance value was obtained because of the repulsion between negative charge of MB decorated DNA strand and $[Fe(CN)_6]^{3-/4-}$ anions (curve f). These above results verified that the PEC biosensor was assembled as expected.

3.3. Optimization of experimental conditions

To obtain a better analytical performance for PEC biosensor, several experimental parameters, containing the concentration of photoelectric material PTCDA, the concentration of hole-trapping reagent L-Cys and the cleavage time of Mg^{2+}, were evaluated at an invariable Mg^{2+} concentration (100 nM). Increasing the concentration of photoelectric material PTCDA in a certain range was beneficial to improve the absorption of light. However, with the increase of PTCDA concentration, the steric hindrance gradually enhanced, which could hinder the electron transfer to a certain extent. As exhibited in Fig. 2A, the photocurrent response of PTCDA modified electrode continuously enhanced with increasing concentrations of PTCDA from 1 to 4 mM and then began to stabilize. Consequently, 4 mM PTCDA was utilized as optimal concentration of photoelectric material.

As an electron donor, increasing the concentration of L-Cys was conductive to reduce the electron-hole recombination rate. However, since the number of electrons and holes generated by the electrode was constant under inevitable conditions, the excess electron donor beyond this range would not further promote electron transfer. Therefore, the majorizing concentration of L-Cys was studied in the range from 10 mM to 100 mM with PTCDA/GCE. As depicted in Fig. 2B, the PEC signal enhanced with incremental concentrations of L-Cys from 10 to 80 mM and then reached plateau when the concentration of L-Cys exceeded 80 mM. Accordingly, PBS containing 80 mM L-Cys was applied as the best detection buffer. Moreover, the amount of Fc largely depended on cleavage time of Mg^{2+}. As shown in Fig. 2C, the photocurrent signal of Fc-S2/β-CD/depAu/PTCDA/GCE decreased gradually with the augment of time and then leveled off at 120 min. Fig. 2D was the corresponding photocurrent at different cleavage time of Mg^{2+}. As the cleavage time of Mg^{2+} increased, the PEC signal gradually decreased within 60 to 120 min, and then tended to be steady. Thus, 120 min was the optimal cleavage time of Mg^{2+} in the DNA recycle.

3.4. Analytical performance of PEC multiple system

To evaluate the analytical performance of as-devised PEC multiple assay, the quantitative measurement was utilized by detecting various concentrations of Mg^{2+} and Pb^{2+}. Fig. 3A represented the PEC intensity change with increasing concentration of Mg^{2+} in the range from 1 pM to 100 nM at the excitation wavelength of 590 nm. Fig. 3B exhibited the linear regression equation between the PEC values and logarithmical (lg) concentrations of Mg^{2+}, which has been wrote as

$$I_1 = -0.0471 \lg c_{Mg2+} + 0.68041, (590\ nm)$$

where I_1 represented the PEC values (μA) at 590 nm, and $c_{Mg}{}^{2+}$

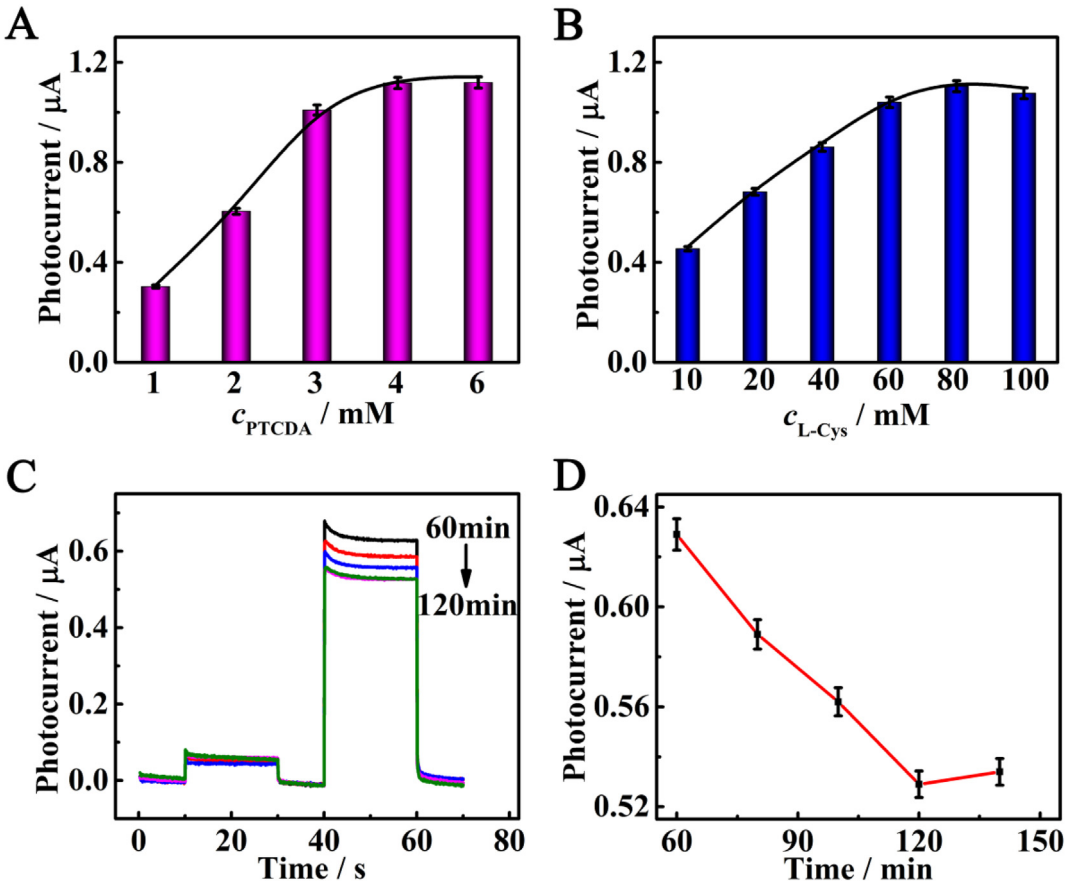

Fig. 2. The optimization of experimental parameters explored by PEC measurement: (A) the effect of PTCDA concentration on PEC initial intensity, (B) the effect of L-Cys concentration on PEC sensor performance, (C) the influence of cleavage time for target Mg^{2+} and (D) the corresponding trend curves at different cleavage time of Mg^{2+}.

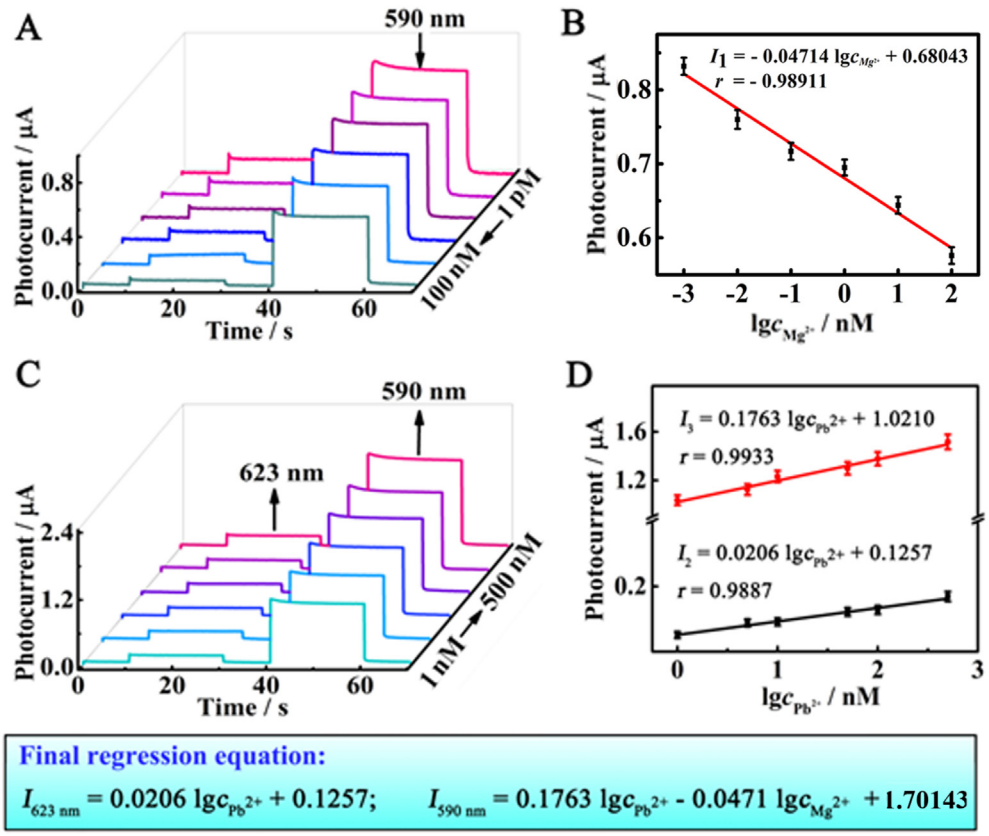

Fig. 3. (A) Photocurrent signal of the biosensor with different concentrations of Mg^{2+} (1 pM, 10 pM, 100 pM, 1 nM, 10 nM, 100 nM). (B) The linear relationship between photocurrent responses and the concentration of Mg^{2+}. (C) Photocurrent signal of the biosensor with different concentrations of Pb^{2+} (1 nM, 5 nM, 10 nM, 50 nM, 100 nM, 500 nM). (D) The linear relationship between photocurrent responses and the concentration of Pb^{2+}.

indicated the concentration (pM) of Mg^{2+}. Fig. 3C showed the PEC signals variation with increasing concentration of Pb^{2+} in the range from 1 nM to 500 nM at 623 nm and 590 nm, respectively. Fig. 3D was the corresponding linear equation for Pb^{2+}, which could be indicated as

$$I_2 = 0.0206\ \lg c_{Pb2+} + 0.1257,\ (623\ nm)$$

$$I_3 = 0.1763\ \lg c_{Pb2+} + 1.0210,\ (590\ nm)$$

where I_2 represented the PEC values at 623 nm, I_3 represented the PEC values at 590 nm, and c_{Pb2+} indicated the concentration (nM) of Pb^{2+}. We could see that the photocurrent signal at 623 nm was changed only with the variation of Pb^{2+} concentration, while the signal at 590 was affected by both Pb^{2+} and Mg^{2+} concentration. Therefore, taking above formulas into consideration, the final regression equation could be calculated as

$$I_{623\ nm} = 0.0206\ \lg c_{Pb2+} + 0.1257$$

$$I_{590\ nm} = 0.1763\ \lg c_{Pb2+} - 0.0471\ \lg c_{Mg2+} + 1.70143$$

The conceived biosensor for Mg^{2+} and Pb^{2+} detection realized high sensitivity with detection limit of 0.3 pM and 0.3 nM, respectively, which was lower than that of other reports (as shown in Table 1). Thus, this PEC biosensor illustrated excellent sensitivity with a low detection limit, realized the simultaneous multiplex assay on a single sensing platform. Therefore, c_{Mg2+} and c_{Pb2+} could be simultaneously detected with variational PEC signals, which induced by the amount of generated MB-S1 and Fc-S2 after target recognition.

3.5. Selectivity and stability of the PEC biosensor

The selectivity of the constructed PEC biosensor for detecting Mg^{2+} and Pb^{2+} was also explored by measuring other interference ions such as Na^+, K^+, Co^{2+} and Cd^{2+} under the same conditions. As shown in Fig. 4A, these interfering substances had no obvious effect at even 10-fold higher concentration of target, which indicated that our PEC biosensor held good specificity for Mg^{2+} and Pb^{2+}. Meanwhile, as a vital factor in PEC assay, the stability of biosensor was researched upon 5 periodic off-on-off light. As shown in Fig. 4B, the electrode exhibited reproducible responses with negligible decrease for duration of circles, indicating its excellent photoelectric stability. Moreover, the inter-/intra-assay were studied to verify the stability of proposed method. The results suggest that both the PEC signals of intra-assay and inter-assay variation was relatively small and the calculated RSD was 4.6% and 6.9%, respectively (n = 3). Additionally, the storage stability of proposed biosensor was also investigated. The same β-CD/depAu/PTCDA/GCE was investigated by CV every day and stored in refrigerator. The current value just reduced 2.3% compared with that of previous current after 5 days. The superior stability can be ascribed the well membrane-forming property of PTCDA.

4. Conclusion

We have developed a multiplex PEC biosensor based on wavelength distinguishable signal quenching and enhancing toward photoactive material PTCDA for simultaneous assay of Pb^{2+} and Mg^{2+}. The Pb^{2+} and Mg^{2+}-induced DNAzyme-assisted target recycling could significantly increase the output of MB-S1 and Fc-S2 with improved detection sensitivity. Additionally, the well film-forming property of PTCDA enabled the substantial immobilization on electrode, thus avoiding the fussy labeling process and further improving the sensitivity. More importantly, this strategy not only achieved the discrimination of varied PEC signal caused by two targets with usage of sole photoelectric material, but also realized the simultaneous multiplex assay on a single sensing platform. The further study on establishing more effective and sensitive PEC biosensor for simultaneous multiplex assay in the real samples is underway.

Table 1
Comparison for the metal ions detection with other analytical methods.

Analytical method	Detection limit	Detection range	Ref.
Fluorescence	Pb^{2+}: 0.3 nM Cu^{2+}: 1 nM Mg^{2+}: 200 nM	Pb^{2+}: 1 nM–500 nM Cu^{2+}: 2 nM–500 nM Mg^{2+}: 0.5 nM–200 μM	
Surface-enhanced Raman Scattering	Pb^{2+}: 0.99 pM Hg^{2+}: 84 nM	Pb^{2+}: 0.1 nM–10 μM Hg^{2+}: 1 nM–10 μM	Shi et al. (2018)
PEC	Pb^{2+}: 166 pM Mg^{2+}: 34 pM	Pb^{2+}: 500 pM–900 nM Mg^{2+}: 100 pM–1 μM	Deng et al. (2019)
Inductively Coupled Plasma Mass Spectrometry	Cr^{3+}: 4.808 ng L^{-1} Pb^{2+}: 3.401 ng L^{-1}	Cr^{3+}: 0.05 μg L^{-1}–60 μg L^{-1} Pb^{2+}: 0.05 μg L^{-1}–60 μg L^{-1}	Suo et al. (2019)
Electrochemistry	Cr^{3+}: 1 μg L^{-1} Pb^{2+}: 1 μg L^{-1}	Cr^{3+}: 5–150 μg L^{-1} Pb^{2+}: 5–150 μg L^{-1}	Rattanarat et al. (2014)
Fluorescence	Hg^{2+}: 10 nM Ag^{+}: 10 nM Pb^{2+}: 20 nM	Hg^{2+}: 10 nM–200 nM Ag^{+}: 10 nM–400 nM Pb^{2+}: 20 nM–2000 nM	Qu et al. (2017)
PEC	Mg^{2+}: 0.3 pM Pb^{2+}: 0.3 nM	Mg^{2+}: 0.001–100 nM Pb^{2+}: 1–100 nM	**This work**

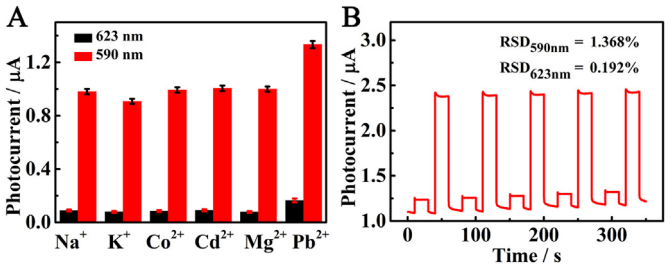

Fig. 4. (A) Selectivity of the proposed PEC biosensor toward Na^+ (5 μM), K^+ (5 μM), Co^{2+} (5 μM), Cd^{2+} (5 μM), Mg^{2+} (100 nM), and Pb^{2+} (500 nM). (B) The PEC stability of well-designed biosensor with 100 nM Pb^{2+} under repeated on/off illumination cycles.

Credit author statement

All authors have given approval to the final version of the manuscript.

CRediT authorship contribution statement

Liaojing Huang: Conceptualization, Data curation, Formal analysis, Investigation, Writing - original draft, Writing - review & editing. **Hanmei Deng:** Data curation, Investigation. **Xia Zhong:** Conceptualization, Writing - original draft, Supervision. **Minghui Zhu:** Conceptualization, Writing - original draft, Supervision. **Yaqin Chai:** Conceptualization, Writing - original draft, Supervision. **Ruo Yuan:** Resources, Project administration, Supervision. **Yali Yuan:** Funding acquisition, Resources, Writing - review & editing.

Declaration of competing interest

The authors declare that they have no known competing financial interests or personal relationships that could have appeared to influence the work reported in this paper.

Acknowledgements

This work was supported by the Chongqing Research Program of Basic Research and Frontier Technology (cstc2018jcyjA0797), the Fundamental Research Funds for the Central Universities (XDJK2019B022, SWU117045, XDJK2018C041), and the National Natural Science Foundation (NNSF) of China (51473136, 21575116).

Appendix A. Supplementary data

Supplementary data to this article can be found online at https://doi.org/10.1016/j.bios.2019.111702.

References

Agnihotri, N., Chowdhury, A.D., De, A., 2015. Biosens. Bioelectron. 63, 212–217.
Bar-Shir, A., Yadav, N.N., Gilad, A.A., van Zijl, P.C.M., McMahon, M.T., Bulte, J.W.M., 2015. J. Am. Chem. Soc. 137, 78–81.
Chen, L.F., Tian, X.K., Xia, D.S., Nie, Y.L., Lu, L.Q., Yang, C., Zhou, Z.X., 2019. ACS Omega 4, 5915–5922.
Dai, H., Zhang, S.P., Hong, Z.S., Lin, Y.Y., 2016. Anal. Chem. 88, 9532–9538.
Deng, H.M., Huang, L.J., Chai, Y.Q., Yuan, R., Yuan, Y.L., 2019. Anal. Chem. 91, 2861–2868.
Frens, G., 1973. Nat. Phys. Sci. 241, 20–22.
Guo, X.X., Liu, S.P., Yang, M.H., Du, H.T., Qu, F.L., 2019. Biosens. Bioelectron. 139, 111312.
Huang, L.J., Yang, L., Zhu, C.C., Deng, H.M., Liu, G.P., Yuan, Y.L., 2018a. Sens. Actuators B Chem. 274, 458–463.
Huang, L.J., Zhang, L., Yang, L., Yuan, R., Yuan, Y.L., 2018b. Biosens. Bioelectron. 104, 21–26.
Jiang, J.J., Lin, X.Y., Ding, D., Diao, G.W., 2018. Biosens. Bioelectron. 114, 37–43.
Li, F.L., Guo, Y.M., Wang, X.Y., Sun, X., 2018. Biosens. Bioelectron. 115, 7–13.
Li, L., Fan, Y.Y., Li, Q.L., Sheng, R.J., Si, H.B., Fang, J., Tong, L.L., Tang, B., 2017. Anal. Chem. 89, 4559–4565.
Li, L., Feng, J., Fan, Y.Y., Tang, B., 2015. Anal. Chem. 87, 4829–4835.
Liu, X., Zhu, Z.L., Bao, Z.Y., He, D., Zheng, H.T., Liu, Z.F., Hu, S.H., 2019. Anal. Chem. 91, 928–934.
Lu, M.X., Deng, Y.J., Luo, Y., Lv, J.P., Li, T.B., Xu, J., Chen, S.W., Wang, J.Y., 2019. Anal. Chem. 91, 888–895.
Miao, P., Tang, Y.G., Wang, L., 2017. ACS Appl. Mater. Interfaces 9, 3940–3947.
Qu, X.M., Yang, F., Chen, H., Li, J., Zhang, H.B., Zhang, G.J., Li, L., Wang, L.H., Song, S.P., Tian, Y., Pei, H., 2017. ACS Appl. Mater. Interfaces 9, 16026–16034.
Rattanarat, P., Dungchai, W., Cate, D., Volckens, J., Chailapakul, O., Henry, C.S., 2014. Anal. Chem. 86, 3555–3562.
Shen, C., Ge, S.Y., Pang, Y.Y., Xi, F.N., Liu, J.Y., Dong, X.P., Chen, P., 2017. J. Mater. Chem. B 5, 6593–6600.
Shi, Y., Chen, N., Su, Y.Y., Wang, H.Y., He, Y., 2018. Nanoscale 10, 4010–4018.
Suo, L.Z., Zhao, J., Dong, X.Y., Gao, X.Z., Li, X.Z., Xu, J.F., Lu, X.M., Zhao, L.S., 2019. New J. Chem. https://doi.org/10.1039/C9NJ02038A.
Tang, W.X., Wang, Z.Z., Yu, J., Zhang, F., He, P.G., 2018. Anal. Chem. 90, 8337–8344.
Tassali, N., Kotera, N., Boutin, C., Léonce, E., Boulard, Y., Rousseau, B., Dubost, E., Taran, F., Brotin, T., Dutasta, J.P., Berthault, P., 2014. Anal. Chem. 86, 1783–1788.
Wang, J., Liu, Z.H., Hu, C.G., Hu, S.S., 2015. Anal. Chem. 87, 9368–9375.
Wang, J., Long, J., Liu, Z.H., Wu, W.Z., Hu, C.G., 2017. Biosens. Bioelectron. 91, 53–59.
Wang, Y.H., Ning, G., Wu, Y.H., Wu, S., Zeng, B.Q., Liu, G.Q., He, X.X., Wang, K.M., 2019. Biosens. Bioelectron. 124–125.
Wang, Z.K., Gong, X., Li, M., Hu, Y., Wang, J.M., Ma, H., Liao, L.S., 2016. ACS Nano 10, 5479–5489.
Wu, S.S., Wei, M., Wei, W., Liu, Y., Liu, S., 2019. Biosens. Bioelectron. 129, 58–63.
Yang, R.Y., Zou, K., Zhang, X.H., Du, C.C., Chen, J.H., 2019. Biosens. Bioelectron. 132, 55–61.
Yun, W., Wu, H., Liu, X.Y., Fu, M., Jiang, J.L., Du, Y.F., Yang, L.Z., Huang, Y., 2017. Anal. Chim. Acta 986, 115–121.
Zeng, R.J., Luo, Z.B., Su, L.S., Zhang, L.J., Tang, D.P., Niessner, R., Knopp, D., 2019a. Anal. Chem. 91, 2447–2454.
Zeng, R.J., Zhang, L.J., Luo, Z.B., Tang, D.P., 2019b. Anal. Chem. 91, 7835–7841.
Zhang, L.J., Luo, Z.B., Zeng, R.J., Zhou, Q., Tang, D.P., 2019. Biosens. Bioelectron. 134, 1–7.
Zheng, Y.N., Liang, W.B., Yuan, Y.L., Xiong, C.Y., Xie, S.B., Wang, H.J., Chai, Y.Q., Yuan, R., 2016. Biosens. Bioelectron. 81, 423–430.
Zhu, Y.C., Xu, Y.T., Xue, Y., Fan, G.C., Zhang, P.K., Zhao, W.W., Xu, J.J., Chen, H.Y., 2019. Anal. Chem. 91 (10), 6419–6423.
Zhuang, J.Y., Lai, W.Q., Xu, M.D., Zhou, Q., Tang, D.P., 2015. ACS Appl. Mater. Interfaces 7, 8330–8338.